JJMIE

Volume 18, Number 4, November. 2024
ISSN 1995-6665
Pages 661- 669
https://doi.org/10.59038/jjmie/180403
Editor-in-Chief: Prof. Ali M. Jawarneh

Jordan Journal of Mechanical and Industrial Engineering

Microstructural properties and Adhesive Strength of 316L Stainless Steel Coated with Hydroxyapatite Derived from Mussel Shell Wastes via Flame Spray Deposition

Muh Amin [1,2], Rifky Ismail [1,3], J. Jamari [1], Athanasius P. Bayuseno [1,*]

[1] Department of Mechanical Engineering, Faculty of Engineering, Diponegoro University, Tembalang, 50275, Semarang, Indonesia
[2] Department of Mechanical Engineering, Universitas Muhammadiyah Semarang, Kedungmundu, Semarang 50273, Indonesia
[3] Center for Bio Mechanics, Bio Materials, Bio Mechatronics and Bio Signal Processing (CBIOM3S), Diponegoro University, Semarang, Indonesia University, Salt, Jordan. 16310

Received 23 Apr 2024 *Accepted 19 Aug 2024*

Abstract

316L stainless steel (316L SS) is an excellent implant material because of its durability, low modulus, superior corrosion resistance, and biocompatibility. However, 316L SS was bioinert and cannot be combined with living tissue. To cover this weakness, 316L SS needs to be coated with a material that has high bioactivity, such as hydroxyapatite (HA) bioceramic. Flame spray deposition (FSD) is a promising method for applying hydroxyapatite to 316L SS, but the deposition product's low interfacial adhesion makes it brittle. This study recommends preheating the substrate (300, 600, and 900) C to improve the adhesive bond before coating it with hydroxyapatite. The coated 316L SS product was then subjected to mechanical testing and analytical techniques (XRD and SEM/EDX) to evaluate its osseointegration, microstructures, and adhesive strength. After preheating to 900°C, the resulting coated steel showed a significant increase in adhesion strength. The crystallinity index also increased to 99.35%. However, the porosity and layer thickness decreased. The current work can shed light on the coating procedure for stainless steel, which is a promising material for implants, and it can also guide future investigations into the potential uses of HA made from mussel wastes.

Keywords: Adhesive strength; Coating; Flame spray deposition; Hydroxyapatite; Mussel shell wastes; Stainless steel.

1. Introduction

Metal implants are preferred as internal fixation to help the bone healing process. [1]. Metal alloys such as 316L (SS) stainless steel [2], titanium [3], and titanium alloys [4] are frequently utilized for orthopedic implants [5]. In particular, the 316L SS alloy is well-suited for replacing damaged bone due to its high strength, non-toxicity, biological compatibility, low density, and fatigue resistance [6, 7]. However, 316L SS implanted in the body can cause biocorrosion and release toxic ions such as Fe, Cr, and Ni into human tissue [8], resulting in pain and a longer healing time. Additionally, the bioinert nature of 316L SS, which inhibits osteogenesis, is a concern for its application [9]. Applying a bioceramic coating to a metal surface improves osteoconductivity and increases its clinical durability. The biomaterial design of the interface makes it appealing to incorporate a biocompatible coating into orthopedic prostheses [10]. One of the materials used in bioactive coatings is hydroxyapatite (HA) [$Ca_{10}(PO_4)_6(OH)_2$]. Coating metal alloys with hydroxyapatite can enhance implant fixation and stability. As a result, the HA coating can react to its physiochemical environment and adapt as needed, resulting in high bioactivity and prolonged osteoconduction. Hydroxyapatite forms a chemical bond with the surfaces of metal implants and natural bone due to its similar mineral composition, crystalline structure, and chemical makeup[11].

Further, coating 316L SS with HA can help improve its biocompatibility and osseointegration. This condition makes the chemical elements of the coated sample have high biocompatibility [12]. Most biomaterials in biomedical applications composed of Ca/P material closely resemble the natural bone mineral phases. In tooth enamel (~90%) and bone (~60%), calcium/phosphorus are the main inorganic components [13]. In particular, flame-sprayed biomaterial coatings using hydroxyapatite show potential as drug delivery systems due to their large surface area and pore volume. [14]. It also enhanced bone growth. Although HA powder coating improved the biological response and corrosion resistance of 316L SS, it also resulted in low bond strength and surface cracking [15]. The adhesion strength and surface properties of 316L SS substrates coated with HA can be enhanced using various methods [16–19].As a result, the current study has focused on developing novel approaches for the deposition of HA coatings to reduce microcrack problems and optimize coating properties. Out

* Corresponding author e-mail: apbayuseno@gmail.com, r.ismail.undip@gmail.com.

of all the deposition techniques, the US Food and Drug Administration (FDA) has only approved FSD (flame spray deposition) as a HA coating technique for biomedical implants [20]. The FSDmethod has an excellent deposition rate, inexpensive investment costs, economical operating costs, and a relatively simple repair process [21]. The FSD on metallic titanium raises the specific surface area on the substrate coated with HA, leading to increased cell proliferation. Experimental FSD for HA coating onto metal implants revealed that in vitro specimens had increased cell attachment and alkaline phosphatase (ALP) activity [20]. This HA spraying technique, known as wet coating, can result in biologically active bone regeneration implants [20].

Recent scientific advances and clinical case reports have shed more light on the mechanisms that underpin HA coatings. A critical component missing from this foundational study is the relationship between the processing parameters used to form biomaterial coatings and the performance achieved[22 - 24]. The following are the main questions that need to be answered: (1) how the so-formed phase structure relates to the thermal spray devices and manufacturing parameters; (2) how thermal spray methods can be limited to create an appropriate HA coating that might display specific functionalities; (3) how thermal spray methods can create specific phases and what the importance of positioning these phases at specific locations within the coating is; and (4) how the number of pores can be controlled during the manufacturing process.

In practice, solid, semi-molten, or molten bioceramic particles are sprayed onto a metallic substrate using thermal spraying. The particles must move quickly enough to cause plastic deformation when they come into contact with the substrate to form successful coatings. Moreover, a carrier gas stream serves to heat and accelerate the particles. By mixing gaseous fuel with oxygen, flame spraying is a type of thermal spraying that creates a flame. The range of flame temperatures is 3000–3350 K [21]. The deposition of zinc-doped HA onto a Ti-6Al-4V alloy substrate has been demonstrated through flame spraying. According to Mehrvarz et al.[23], the deposit was antibacterial and biocompatible with E. coli. AISI 316L stainless steel and Ti6Al4V alloy substrates were coated with bioactive glass coatings by Monsalve et al. [25] via flame spraying. This condition makes the coated sample have high biocompatibility. Even though the coating surfaces develop an apatite layer in a simulated biological fluid, the coatings may exhibit numerous cracks caused by residual stresses from the coatings' rapid cooling. Preheating before the coating process should reduce the differences in thermal expansion coefficients between the coatings and substrates [13]. In this case, slower cooling rates following thermal spraying can relieve residual stresses and prevent cracking.

In this study, the application of HA flame spray coating to 316L SS implant material was examined through the use of optical analysis, X-ray diffractometry (XRD), and scanning electron microscopy (SEM-EDX). The study concentrated on the preheating temperature response to enhance the HA-coated 316L substrate's adhesion strength, microstructure, Ca/P, crystallinity index, and layer thickness. This study may improve our understanding of using the FSD method to deposit hydroxyapatite on stainless steel for implant bone materials.

2. Materials and methods

2.1. Preparation of powder HA

Green mussel shell (GMS) powder feedstock hydrothermally produced 90–97 wt.% hydroxyapatite powder at 160°C for 18 hours, with crystal sizes ranging from 3 to 10 μm, as previously reported[26].Before applying this powder as a coating on 316L stainless steel, it was dehydrated in an oven for 20 minutes at 150°C and ground in a kaolin mortar to ensure size consistency after sifting the powder between 200-325 mesh.

2.2. HA layer deposition

The SS 316L alloy substrate was cut to 35 mm × 35 mm × 2 mm using wire EDM[27-29], followed by finishing with SiC grid 2000 sandpaper. The substrate was washed in 5 vol.% NaOH [10] as a final step to remove dust, oil, and other contaminants. To increase coating adhesion on the dried surface sandblasted using a NEIKO 30068A Air Sand Blaster Gun with Gravity Feed [30]. The sandblasting process at 100 mm of safe distance used 60 mesh silica granules at a 90-degree angle and an 8-bar pressure for 1.5 minutes for 24 specimens with side dimensions (1.5 x 1.5) cm. The blown samples were cleaned with alkali at a 5% volume percent NaOH and dried. Before coating, the cleaned surface was heated initially by a flame spray gun to ensure proper spreading formation and reduce any remaining stresses.

Further, dry HA powder was sprayed onto a sandblasted 316L SS alloy base using the Flame Spray Paint System (QHT-7/h Oxygen Propane, China). Several experiments have improved the adhesion and quality of the coating by adjusting its conditions (Figure 1). Table 1 describes the optimal process parameters for spraying. LPG gas [31, 32](PERTAMINA weighing 11 kg propane (PR) with design pressure of 18.6 bar) was used as an oxygen-containing combustion gas to transport powder material from the powder feeder to the spray flame. Gas pressure has the greatest effect followed by the interaction between gas pressure and stand off distance in thermal spray coating processes [33,34]. The spraying process involved five passes by each with the HA powder delivery head open at a 45-degree angle. The varying preheating temperatures present are in Table 2.The raw powder and coating samples were designated GMS.P and GMS.WP, GMS.300, GMS.600, and GMS.900, respectively. Three samples were prepared for each treatment.

2.3. XRD analysis

The study's coating samples, measuring 5 × 5 mm^2 and having a thickness of 2 mm, were prepared for XRD analysis. XRD measurements on the starting powders and the final coating materials are in compliance with ISO Standard 13779-3:2008 [35]. The X-ray diffraction pattern recorded used the diffractometer (Bruker Corporation, Massachusetts, USA) with monochromatic Cu-Kα radiation (λ= 0.15406 nm) in the Bragg Brentano mode (10-80^{O} 2θ; 0.022^{O}/step and 30-second/step) at 40kV and 30 mA. Moreover, *QualX-PC*-search-match software helped to identify XRD phases in the coating product associated with

the COD# (Crystallography Open Database) crystallographic model [36]. Afterward, using Program *X'Pert* plus version 1.0 (Philip Analytical, BV) and the COD#data, the Rietveld refinement method confirmed the crystalline phases found by the search match method. Instead, the deconvolution of the X-ray diffractogram using the software Match and Origin Lab 9.0 determined amorphous and crystalline phases and calculated the percentage of the crystallinity of the HA layer. The crystallite index of the sprayed coating product was calculated based on equation (1), as previously reported [37].

$$X_c = \frac{A_{cr}}{A_{cr} + A_{am}} x100\% \quad (1)$$

2.4. Morphological and elemental chemical analysis

The flame-sprayed samples were examined microstructurally by standard metallographic procedures. An optical microscope (METKON-IMM 902) was employed to evaluate the microstructure of the surface samples, as well as analysis using a scanning electron microscope (SEM) equipped with an energy-dispersive X-ray (EDX) device (JSM-IT700HR InTouchScopeTM) in the scattered electron mode at 15 kV. Furthermore, EDX analysis determined the Ca/P ratio in the layered sample. Instead, image analysis techniques selected SEM images of the coating surface to measure its porosity. The area fractions of multiple pores in the coating were employed to calculate the average percentage of porosity. The average porosity calculation used images captured at various locations.

2.5. Tensile adhesion strength analysis

The ASTM D4541 standard is used to determine the tensile adhesive strength of specimens using a PosiTest AT-A Automatic test equipment. HA from GMS was applied to square-shaped samples (gauge length 35 mm, width 35 mm, and nominal thickness 2 mm) at different pre-heating temperatures. Blue Araldite was used to attach a dolly with a diameter of 25.4 mm to the HA coating layer. After thoroughly cleaning the substrate containing the HA layer and the dolly surface, the sample was allowed to dry at room temperature for at least 24 h before being glued with a 1:1 volume ratio of hardener and epoxy and agitated for 5 minutes at 54 rpm. After that, use a pile drill to remove any excess glue accumulating on the outside dolly surface. The sample's adhesive strength was tested by detaching the dolly from the substrate at room temperature and 0.5 mm of strain per minute.

Table 1. FSD process parameters for layer deposition

Flame spray parameters	Values
Acetylene pressure (Bar)	2
Oxygen pressure (Bar)	0.5
Distance of spray gun (mm)	100
Preheat temperature (ºC)	300, 600, and 900
Nozzle size of spray gun (mm)	2
Number of passes	5

Table 2. Preheat temperature settings used in this work

Abbreviation	**Description**	**Range of operating temperature (ºC)**
GMS.P	Powder	-
GMS.WP	Without preheat	100-200
GMS.300	Preheat 300ºC	300-350
GMS.600	Preheat 600ºC	600-650
GMS.900	Preheat 900ºC	900-950

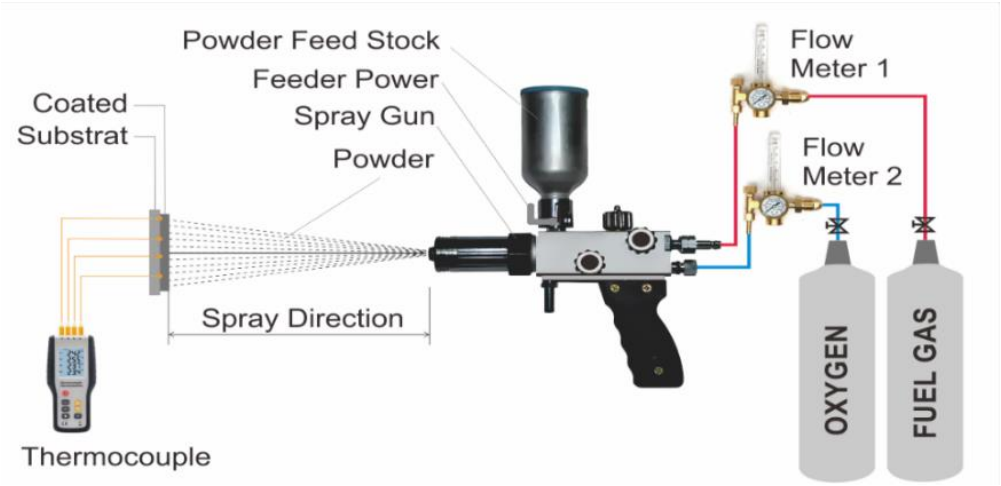

Figure 1. HA coating process on 316L SS

3. Result and discussion

3.1. XRD analysis

Figure 2 depicts the XRD spectra of the powder feedstock and the GMS coating samples. The findings show that the starting powder samples contain the main crystal of hydroxyapatite structures (COD#number data_9010050). The hump background reflection indicates that the hydroxyapatite powder sprayed on the substrate may produce amorphous calcium phosphates (ACP). Whether the metallic substrate was heated previously or not, the coating results still revealed the presence of the HA pattern, as seen in all GMS-coating samples with reducing diffraction peaks, confirming an ACP present, which resulted in a broad reflection cantered at approximately 30-40^{O} 2θ. The HA product undergoes thermal breakdown during the flame spraying processes, becoming molten and creating an amorphous phase. As a result, the coating products have multiple phase compositions, including an amorphous phase, as shown by XRD patterns of GMS.P and GMS.WP, GMS.300, GMS.600, and GMS.900 specimens. In contrast, samples GMS.900 confirm 316L SS phase diffraction peaks in addition to the weak peaks seen in other coating specimens, indicating that the all-surface coating does not cover the hydroxyapatite or the presence of porous specimens.

3.2. Macro-and microstructure characterization

The macro description of the surface morphology of the HA layer scale (Fig. 3) supports a rough and porous macrostructure of the coated HA layer, consisting of multiple agglomerated micro-sized particles of different sizes and spherical fragments. The fully-melted HA particles associated with the smoother surfaces are also supported.

Figure 4 shows SEM images of the HA layer's surface morphology after spray coating. Observable surface characteristics include spherical particles and tiny nodules connected to completely melted stains. Spherical particles on the surface may be un-melted or partially melted particles. With a porosity of 1 to 5 µm, the spherical particles for all coating specimens have a size range of 0.2 to 2 µm. In particular, the HA coating specimen of GMS.600 exhibited micro-surface cracks (Fig. 4c). In this case, at a higher preheat temperature (600^{o} C), metal elements such as Fe, Cr, and Ni appear in the HA layer, resulting in a single phase (Fig. 4c). The strength of this single phase increases as the preheat temperature rises.

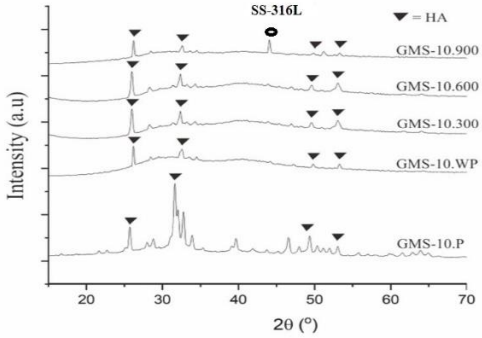

Figure 2.XRD patterns of GMS-coated samples

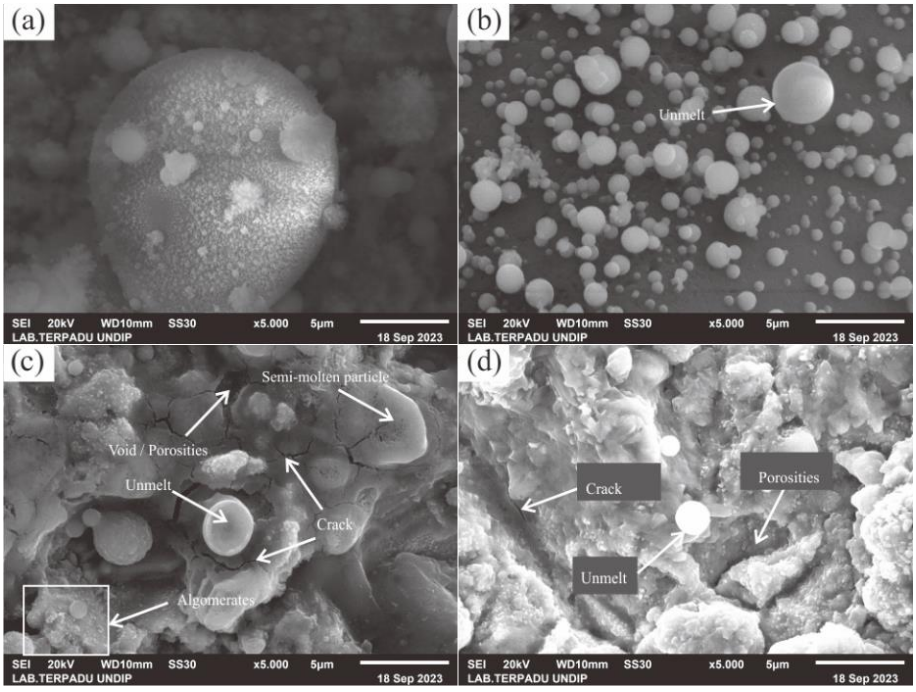

Figure 3. HA surface morphology of GMS layers at various preheat temperatures (a) Without preheat; (b) Preheat at 300ºC; (c) Preheat at 600ºC; (d) Preheat at 900ºC

Microcracks on the surface may be caused by the rapid cooling process used in flame spraying and thermal expansion of metals [38,39]. However, at a preheat temperature of 900º C, the visible cracks on the layer's surface decreased. The solidification process of the HA layer at low preheating temperatures entails cooling two different materials (316L SS and HA) with different thermal coefficient expansion. At a preheat temperature of 900ºC, the incompletely coated HA on the surface substrate made the concentration of Fe, Cr, and Ni elements emerge on its surface (Fig. 4c). This means that the HA layer along with preheat at 900º C have 316L SS metal elements. As a result, a thermal gradient between the HA and 316L SS boundaries can produce a more uniform temperature decrease. Microcracks in the surface HA coating may appear as a result of rapid cooling. To avoid cracking on the surface coating after thermal spraying is required by slower cooling rate to reduce residual stresses while minimizing the difference in coefficient of thermal expansion between the coating and the substrate [20]. Microstructural flaws in the coating, such as microcracks, can cause the substrate to come into direct contact with body fluids, causing damage to the coating. This condition results in layer damage via delamination and fragmentation [40].

Furthermore, EDX analysis at a specific location in each sample (Figs. 4a-d) reveals chemical elements such as Ca, P, O, and C correspond to calcium phosphate mineral compositions. The elements O, Ca, and P, which are the dominant elements of human bones, increased along with the increase in preheat temperature from 35.34%, 14.28, 6.80% to 51.9%, 22.79%, 12.87% respectively. Carbon seems to relate to the carbonic gas created when calcium carbonate, known as CAP (calcium carbonate-apatite), is sprayed with a flame. Additionally, EDX spectra for Cr, Fe, Ni, Al, and Mg appear in the surface layers of SS-316 L, indicating that the HA layer was porous. Table 3 also shows the average Ca/P ratios of hydrothermal products from three different locations, with statistical errors ranging from 1.77 to 6.10, indicating that flame spray processes produced more mineral phases than hydroxyapatite, which had a stoichiometrically Ca/P ratio of 1.67 [41].

The Ca/P ratio determined by EDX analysis is not a reliable indicator of the precise crystalline structure formed. This EDX analysis's variations in the Ca/P molar ratios are most likely the result of a microcrack and the presence of an amorphous crystal. Upon closer inspection, the micro-meter sized irregularly agglomerated particles showed morphology similar to that of natural HA powder (Figs. 3a-b), suggesting the presence of un-melted HA particles in the coating. In contrast, the HA layer had a porous surface with spherical fragments and macroscopic particle agglomeration (Figs. 4c, d), with partially melted particles deformed.

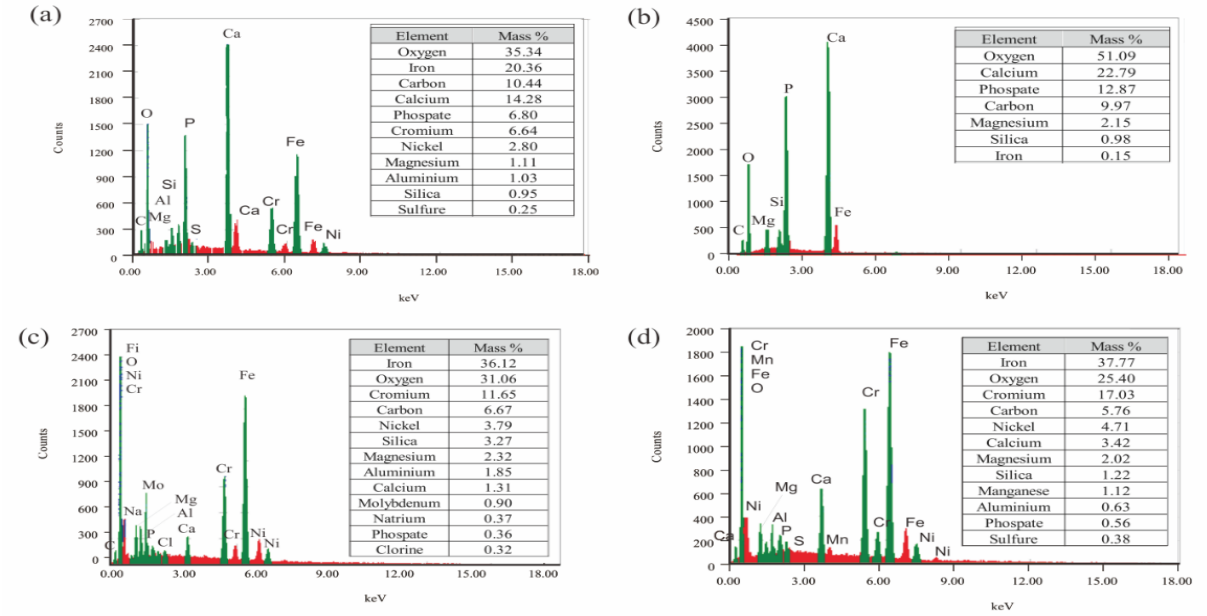

Figure 4. Mapping of HA deposition elements from GSM on substrates at various preheating temperatures (a) Without preheat; (b) Preheat at 300ºC; (c) Preheat at 600ºC; (d) Preheat at 900ºC.

Table 3. Elemental analysis of products using EDX

Atomic concentration (%)	Sample			
	GMS.WP	GMS.300	GMS.600	GMS.900
C	10.44	9.97	6.67	5.76
O	35.34	55.09	31.06	25.40
P	6.80	12.87	0.36	0.56
Ca	14.28	22.79	1.31	3.42
Ratio Ca/P	2.1	1.77	3.63	6.10

3.3. Characterization of the sprayed coating

Observing the macro structure with Image J software can identify phases based on the resolution of all parts of the image. The difference in image resolution in one specimen image is used as a reference for calculating the specimen porosity. Figure 3 shows the porosity specimens which support the SEM observations. The specimen's porosity decreases with increasing preheating temperature. The coating's porosity and thickness are determined by the substrate's preheat temperature and the HA powder used (Fig. 5).

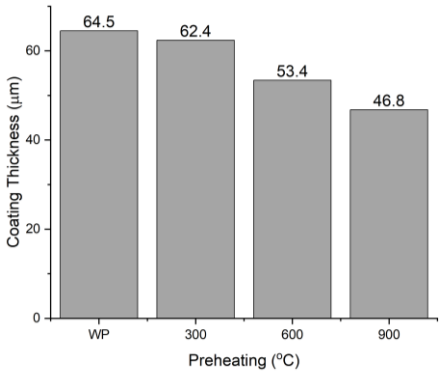

Figure 5. Thickness of HA coated GMS.WP; GMS.300; GMS.600; GMS.900 specimens

The preheat temperature has a significant effect on the porosity of the HA layer. Increasing the preheat temperature gradually reduces the porosity of the HA layer. Similarly, the thickness of the HA layer decreases with increasing preheat temperature [41], with an average layer thickness of 56.77 µm. The thickness of the HA coating on 316L stainless steel for implants varies depending on the coating method and the study. A HA layer typically has a thickness of 50-200 µm [10]. Another study reported that thinner coatings had better bonding between HA powders than thicker coated samples (approximately 72 µm) [42], with the maximum HA layer thickness being 96.76 µm [10]. The thickness of the HA layer can affect the implant's corrosion resistance [42]. However, it is important to note that implant performance is influenced by more than just the thickness of the HA coating. Other factors, such as substrate type and coating method, can also affect the implant's mechanical properties [43]. The degree of crystalline phase formed in the final layer is related to a surface coating layer's crystallinity, which has been considered a significant factor. In the initial stages of bone healing, the HA coating on metal implants can promote strong bone union and enhance osseointegration [44]. The crystallinity of the coating has increased by more than 50% for all coatings. This cristalinity index increases as the preheating temperature increases Fig. 6). As such, the flame spray coating process has prioritized the crystallinity phase of the HA layer. By making the HA coating on metal implants more crystallinity, adhesive bond strength and osteogenic qualities can be improved [45].

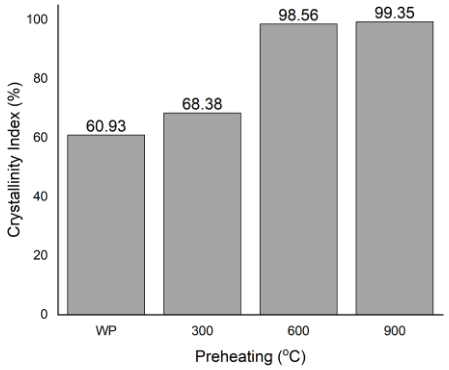

Figure 6. Crystallinity index of HA coated GMS.WP; GMS.300; GMS.600; GMS.900 specimens

3.4. Coating adhesion strength

Figure 7 shows the adhesive strength data obtained through a pull-off test by ASTM D4541. The adhesive strength of the coated HA layer on the substrate decreases with increasing pre-heat temperature. The difference in Young's Modulus between the coating material and the substrate could account for this value. About this issue, HA's use in bone implants remains limited due to its brittleness and low toughness [46]. This condition also applies to implant materials such as 316L SS. The Young's modulus of 316L SS is ~193 GPa, compared to approximately 6 GPa for HA, making the HA layer susceptible to failure due to stress shielding (Young's modulus mismatch between HA and substrate, as reported in [47]. These findings confirmed that higher preheating was associated with an increase in the levels of Fe and Cr elements, resulting in increased adhesion strength. However, because the GMS.600 sample (Fig. 3c) contains many macro-sized cracks, its tensile adhesion strength is lower than that of the GMS.300 sample. Sample GMS.900 (preheat 900°C) had the highest tensile adhesion strength of 3.84 MPa.

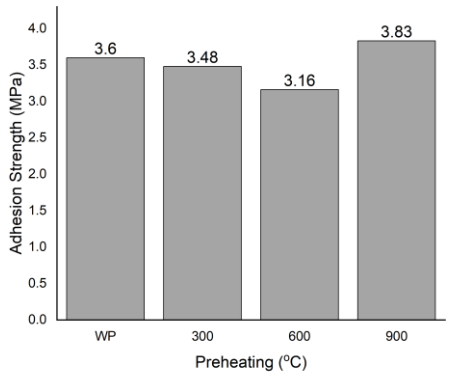

Figure 7. Adhesion strength of HA coated GMS.WP; GMS.300; GMS.600; GMS.900 specimens

According to searches in indexed international journals, the standard adhesion strength of HA coatings on orthopaedics implants depends upon several factors, including the type of coating and substrate material. The adhesion strength of HA coatings on orthopaedics implants

can range from 3.15 MPa to 19.02 MPa, depending on the conditions and materials used [48-49]. Higher adhesive strength indicates increased adhesion between the prosthesis, the new periprosthetic tissue, the substrate, and the coating [30]. However, obtaining a high adhesion strength of HA coating is not ideal because the interface adhesion strength of HA-coated implants increases to 7.27 MPa after ten weeks of implantation [49]. In this study, the adesion strength coating is still less than 15 MPa, so further research is needed. A good HA coating must have adequate adhesion strength, few cracks, high hardness, good osteoconduction, no inclusions, and consistent osseointegration [50].

4. Conclusion

The preheating temperature parameters of the FSD process influence the morphology of the HA layer and its adhesion strength, porosity, coating thickness, and crystallinity index. Adhesion strength and crystallinity index increase with initial heating, but porosity and layer thickness are the opposite.The porosity of the HA coating and the coating thickness decreased with increasing preheating temperature from 19.87% to 3.73% and 64.5 um to 46.8 um respectively. The adhesion strength and crystallinity index of the coatingvary. They increase with increasing preheating temperature from 3.6 MPa to 3.83 MPa and 60.93% to 99.35% respectively.

The findings of this study show that the HA layer material meets the porosity, thickness, and crystallinity index requirements for implant coating materials. Meanwhile, the reduced adhesion strength of the HA layer could be related to the appearance of cracks caused by elastic modulus differences between HA and the substrate during the preheating process.

Acknowledgments

The authors would like to thank the Ministry of Education, Culture, Research, and Technology - Directorate General of Higher Education of the Republic of Indonesia for the 2023 postgraduate research grant with contract numbers SP DIPA-023.17.1.690523/2023, 121/E5/pg.02.00.PL/2023, and 449A-10/UN7.D2/PP/VI/2023. We thank the Department of Mechanical Engineering, Faculty of Engineering, Diponegoro University, and Universitas Muhammadiyah Semarang (UNIMUS) for providing us with facilities and infrastructure.

References

[1] A.H.Q. Ayun, J. Triyono, E. Pujiyanto," Optimization of Injection Molding Simulation of Bioabsorbable Bone Screw Using Taguchi Method and Particle Swarm Optimization". Jordan Journal of Mechanical and Industrial Engineering, Vol. 16, No. 2, 2022, pp. 319 - 325.

[2] K.A. Kravanja, M. Finšgar, "A review of techniques for the application of bioactive coatings on metal-based implants to achieve controlled release of active ingredients". Materials & Design, Vol. 217, 2022, 110653.

[3] J.A. Lenis,E.C. Romero, A.H. Macías, P. Rico, J.L.G. Ribelles, M.A.P. Olivenza, M.L.G. Martín, F.J. Bolívar, "Mechanical, structural, and biological evaluation of multilayer HA-Ag/TiO_2/TiN/Ti coatings on Ti6Al4V obtained by magnetron sputtering for implant applications". Surface and Coatings Technology, Vol. 449, 2022, 128925.

[4] Q. Khalid Naji, J.M. Salman, N.M. Dawood, "Investigations of structure and properties of layered bioceramic HA/TiO_2 and ZrO_2/TiO_2 coatings on Ti-6Al-7Nb alloy by micro-arc oxidation". Materials Today: Proceedings, Vol. 61, 2022, 786–793.

[5] D. Singh, R. Singh, K.S. Boparai, I. Farina, L. Feo, A.K. Verma, "In-vitro studies of SS 316 L biomedical implants prepared by FDM, vapor smoothing and investment casting". Composites Part B: Engineering, Vol. 132, 2018, 107–114.

[6] A. Bekmurzayeva, W.J. Duncanson, H.S. Azevedo, D. Kanayeva, "Surface modification of stainless steel for biomedical applications: Revisiting a century-old material". Materials Science and Engineering: C, Vol. 93, 2018, 1073–1089.

[7] A.H. Haleem, N.S. Radhi, N.T. Jaber, Z.A. Khafaji, "Preparation and Exploration of Nano-Multi-Layers on 316l Stainless Steel for Surgical Tools". Jordan Journal of Mechanical and Industrial Engineering, Vol. 18, No. 2, 2024, pp. 339 - 350. https://doi.org/10.59038/jjmie/180207

[8] M. Li, J. Wu, W. Geng, Y. Yang, X. Li, K. Xu, K. Li, Y. Li, Q. Duan, P. Gao, K. Cai, "Regulation of localized corrosion of 316L stainless steel on osteogenic differentiation of bone morrow derived mesenchymal stem cells". Biomaterials, Vol. 301, 2023, 122262.

[9] A.C. Parau, G.A. Juravlea, J.Raczkowska, C.Vitelaru, M. Dinu, K. Awsiuk, D.M. Vranceanu, E. Ungureanu, C.M. Cotrut, A. Vladescu, "Comparison of 316L and Ti6Al4V biomaterial coated by ZrCu-based thin films metallic glasses: Structure, morphology, wettability, protein adsorption, corrosion resistance, biomineralization". Applied Surface Science, Vol. 612, 2023, 155800.

[10] B.H.A. Khaqani, N.M. Dawood, "Control Degradation of New Magnesium Alloy by MgF2 Coating for Cardiovascular Applications". Jordan Journal of Mechanical and Industrial Engineering, Vol. 18, No. 2, 2024, pp. 391 - 400. https://doi.org/10.59038/jjmie/180211.

[11] A. Fadli, A. Prabowo, S.R. Yenti, F. Huda, A.A. Liswani, D.L. B. Hutauruk, "High performance of coating hydroxyapatite layer on 316L stainless steel using ultrasonically and alkaline pretreatment". Journal of King Saud University - Science, Vol. 35, No. 5, 2023,102681.

[12] M.A. Amin, A.M.A. Rani, M. Rana, S. Hastuty, M. Danish, S. Rubaiee, A.B. Mahfouz, "Evaluation of modified 316L surface properties through HAp suspended EDM process for biomedical application". Surfaces and Interfaces, Vol. 28, 2022, 101600.

[13] H.A. Said,H. Mabroum, M. Lahcini, H. Oudadesse, A. Barroug, H.B. Youcef, H. Noukrati, "Manufacturing methods, properties, and potential applications in bone tissue regeneration of hydroxyapatite-chitosan biocomposites: A review". International Journal of Biological Macromolecules, Vol. 243,2023, 125150.

[14] T.Y. Liao, A. Biesiekierski, C.C. Berndt, P.C. King, E.P. Ivanova, H. Thissen, P. Kingshott,"Multifunctional cold spray coatings for biological and biomedical applications: A review". Progress in Surface Science, Vol. 97, No. 2, 2022,100654.

[15] M. Danish, M.A. Amin, S. Rubaiee, I.A. Gul, A. Ahmed, M.O. Rahman, C. Zhang, M.B. Yildirim, "Investigation of coated 316L steel surface: Surface morphology, composition, corrosion, and biocompatibility using hydroxyapatite mixed-EDM process". Surface and Coatings Technology, Vol. 467,2023, 129689.

[16] B. Minhas,Z. Hanif, M.H. Nadeem, S.A. Batool, K. Ahmad, A. Aizaz, J. Manzur, M.A.U. Rehman, "The electrochemical and in-vitro study on electrophoretic deposition of

chitosan/gelatin/hydroxyapatite coating on 316L stainless steel", Carbohydrate Polymer Technologies and Applications, Vol. 5, 2023, 100322.

[17] P.P. Singh, K. Dixit, N. Sinha, "A sol-gel based bioactive glass coating on laser textured 316L stainless steel substrate for enhanced biocompatability and anti-corrosion properties". Ceramics International, Vol. 48, No. 13, 2022, 18704–18715.

[18] P. Singh, A. Bansal, V. K. Verma, "Hydroxyapatite reinforced surface modification of SS-316L by microwave processing". Surfaces and Interfaces, Vol. 28, 2022, 101701.

[19] B. Garrido, A. Martin-Morata, S. Dosta, I. G. Cano, "Improving the bond strength of bioactive glass coatings obtained by atmospheric plasma spraying". Surface and Coatings Technology, Vol. 470, 2023, 129837.

[20] Y.C. Liu, G.S. Lin, J.Y. Wang, C.S. Cheng, Y.C. Yang, B.S. Lee, K.L. Tung, "Synthesis and characterization of porous hydroxyapatite coatings deposited on titanium by flame spraying". Surface and Coatings Technology, Vol. 349, 2018, 357–363.

[21] K. Sunitha, H. Vasudev, "A short note on the various thermal spray coating processes and effect of post-treatment on Ni-based coatings". Materials Today: Proceedings, Vol. 50, 2022, 1452–1457.

[22] Lech P. The Science and Engineering of Thermal Spray Coatings. 2nd ed. England: John Wiley & Sons Ltd; 2008.

[23] A. Mehrvarz, J.K.Allafi, A.K. Khosrowshahi, "Biocompatibil ityand antibacterial behavior of electrochemically deposited Hydroxyapatite/ZnO porous nanocomposite on NiTi biomedical alloy".Ceramics International,Vol. 48, Issue 11, No. 1, 2022, 16326-16336.

[24] S. Srivastava, S.K. Sarangi, "Fabrication and Testing of Nano Bio-silica, Hemp, and Bamboo Fibre-Reinforced Chitosan Bio-composite Material". Jordan Journal of Mechanical and Industrial Engineering, Vol. 18, No. 2, 2024, pp. 401– 410. https://doi.org/10.59038/jjmie/180212.

[25] M. Monsalve, E. Lopez, H. Ageorges, F. Vargas,"Bioactivity and mechanical properties of bioactive glass coatings fabricated by flame spraying".Surface and Coatings Technology,Vol. 268,2015,142-146.

[26] R. Ismail,T. Cionita, W.L. Shing, D.F. Fitriyana, J.P. Siregar, A.P. Bayuseno, F.W. Nugraha, R.C. Muhamadin, R. Junid, N.A. Endot, "Synthesis and Characterization of Calcium Carbonate Obtained from Green Mussel and Crab Shells as a Biomaterials Candidate". Materials, Vol. 15, 2022, 5712.

[27] M. Soori, M. Asmaela," A Review of the Recent Development in Machining Parameter Optimization". Jordan Journal of Mechanical and Industrial Engineering, Vol. 16, No. 2, 2022, pp. 205 - 223.

[28] S. Bhowmicka, B. Baraia, D. Naikb, S. Sarkara, N. Biswasc, S.K. Maityd, G. Majumdar, "Parametric Study and Optimization of Inconel 625 Processing by ANN and Desirability Function Approach During Graphite Mixed EDM". Jordan Journal of Mechanical and Industrial Engineering, Vol. 17, No. 4, 2023, pp. 625– 643. https://doi.org/10.59038/jjmie/170417.

[29] R.V.S.Subrahmanyam, K. Ramji, P.S. Rao, C,V, Rao," The Analysis of Particle Size Effect on Performance of WC/Cu P/M Compact Sintered Electrode in EDM Process". Jordan Journal of Mechanical and Industrial Engineering, Vol. 15, No. 5, 2023, pp. 451 – 460.

[30] H.M. Ayu, S. Izman, R. Daud, G. Krishnamurithy, A. Shah, S.H. Tomadi, M.S. Salwani, "Surface Modification on CoCrMo Alloy to Improve the Adhesion Strength of Hydroxyapatite Coating". Procedia Engineering, Vol. 184, 2017, 399–408.

[31] G. Prasada, A. Das, " Design Approach of Shell and Tube Vaporizer for LNG Regasification". Jordan Journal of Mechanical and Industrial Engineering, Vol. 12, No. 2, 2018, pp. 109 - 116.

[32] A.S. Mahmood, F.A. Saleh, "Experimental Study of the Effect of Swirl Number and Bluff Body Size on the Stability Map of Premixed LPG Flames in a Tangential Swirl Burner". Jordan Journal of Mechanical and Industrial Engineering, Vol. 17, No. 4, 2023, pp. 595 - 604.https://doi.org/10.59038/jjmie/170414

[33] A. Bashir, A. K. Abdul Jawwad, and K. Abu-Shgair, "Evaluating the Effects of High Velocity Oxy-Fuel (HVOF) Process Parameters on Wear Resistance of Steel-Shaft Materials," Jordan Journal of Mechanical and Industrial Engineering, Vol. 3, Jul. 2009, pp. 157 - 160.

[34] A.P. Irawan, D.F. Fitriyana, J.P. Siregar, T. Cionita, P.T. Anggarina, J.B. Jaafar, R.B. Taqriban, E. Jehadus, J. Manalu, "Influence of Post-Heat Treatment on the Characteristics of FeCrBMnSi Coating on Stainless Steel 304 Substrate Prepared by Twin Wire Arc Spray (TWAS) Method at Various Stand-off Distance". Jordan Journal of Mechanical and Industrial Engineering, Vol. 18, No. 2, 2024, pp. 327 - 337.

[35] A. Altomare, C. Cuocci, C. Giacovazzo, A. Moliternia, R. Rizzia, "QUALX: a computer program for qualitative analysis using powder diffraction data". J. Appl. Cryst., Vol. 41, 2008, 815-817.

[36] E. Tarani, I. Arvanitidis, D. Christofilos, D.N. Bikiaris, K. Chrissafis, G. Vourlias, "Calculation of the degree of crystallinity of HDPE/GNPs nanocomposites by using various experimental techniques: a comparative study". J Mater Sci, Vol. 58, No. 4, 2023, 1621–1639.

[37] J. Huang,S. Zou, W. Xiao, X. Liu, H. Chen, D. Tang, H. Deng, X. Zhou, M. Lei, "Microstructural, mechanical properties and high temperature oxidation of Cr, Al-coated Zr-4 alloy". Nuclear Materials and Energy, Vol. 25, 2020, 100810.

[38] V. P. Lapshin," Analysis of the Effect of Thermal Expansion of Metals on the Stability of the Metal Cutting Process". Jordan Journal of Mechanical and Industrial Engineering, Vol. 17, No. 3, 2023, pp. 345– 355. https://doi.org/10.59038/jjmie/170303.

[39] L. CHELBI, F. HENTATI, A. ZNAIDI," Analysis of Fatigue Life and Crack Growth in Austenitic Stainless Steel AISI 304l". Jordan Journal of Mechanical and Industrial Engineering, Vol. 17, No. 4, 2023, pp. 501– 508. https://doi.org/10.59038/jjmie/170405.

[40] P. Przybilla, E. Subkov, S.H. Latorre, S. Zankovic, H.O. Mayr, A. Killinger, H. Schmal, M. Seidenstuecker, "Effect of 20 µm thin ceramic coatings of hydroxyapatite, bioglass, GB14 and Beta-Tricalciumphosphate with copper on the biomechanical stability of femoral implants". Journal of the Mechanical Behavior of Biomedical Materials, Vol. 144, 2023, 105951.

[41] C.D. Alfarisi, Nurfatihayati, H. Rionaldo, A. Fadli, Komalasari, I. Syafna, L. Arianti, D.L. Lestari, N. Asnila, "The effect of acid treatment and sintering temperature on 316L stainless steel substrate coating with hydroxyapatite". Materials Today: Proceedings, Vol. 87, No. 2, 2023, 259-262.

[42] B. Aksakal, M. Gavgali, B. Dikici, "The Effect of Coating Thickness on Corrosion Resistance of Hydroxyapatite Coated Ti6Al4V and 316L SS Implants". J. of Materi Eng and Perform, Vol. 19, No. 6, 2010, 894–899.

[43] W.S.W. Harun, R.I.M. Asri, A.B. Sulong, S.A.C. Ghani, Z. Ghazalli, "A comprehensive review of hydroxyapatite-based coatings adhesion on metallic biomaterials".Ceramics International, Vol. 44, No. 2, 2018, 1250-1268.

[44] Y.L. Chang, D.Lew, J.B. Park, J.C. Keller, "Biomechanical and morphometric analysis of hydroxyapatite-coated implants with varying crystallinity". J Oral Maxillofac Surg, Vol. 57, No. 9, 1999. 1096–1108.

[45] S. Bose, D. Ke, A.A. Vu, A. Bandyopadhyay, S.B. Goodman, "Thermal Oxide Layer Enhances Crystallinity and Mechanical Properties for Plasma-Sprayed Hydroxyapatite Biomedical Coatings". ACS Appl. Mater. Interfaces, Vol. 12, No. 30, 2020, 33465–33472.

[46] M. Barabashko, A. Ponomarev, A. Rezvanova, V. Kuznetsov, S. Moseenkov, "Young's Modulus and Vickers Hardness of the Hydroxyapatite Bioceramics with a Small Amount of the Multi-Walled Carbon Nanotubes". Materials, Vol. 15, No. 15, 2022, 15155304.

[47] K. Essa, P. Jamshidi, J. Zou, M.M. Attallah, H. Hassanin, "Porosity control in 316L stainless steel using cold and hot isostatic pressing". Materials & Design, Vol. 138, 2018, 21–29.

[48] Y. Duan,S. Zhu, F. Guo, J. Zhu , M. Li, J. Ma , Q. Zhu, "The effect of adhesive strength of hydroxyapatite coating on the stability of hydroxyapatite-coated prostheses in vivo at the early stage of implantation". Arch Med Sci, Vol. 8, No. 2, 2012, 199–208.

[49] W. Akram, R. Khan, M. Petrů, M. Amjad, K. Ahmad, M. Yasir, S. Ahmad, S.S.R. Koloor, "Hydroxyapatite coating for control degradation and parametric optimization of pure magnesium: an electrophoretic deposition technique for biodegradable implants". Journal of Materials Research and Technology, Vol. 26, 2023, 2587–2600.

[50] F.F.R. Pimentel, M.M.M. González, M.G. Rocha, "A short review: hydroxyapatite coatings for metallic implants". Heat Treatment and Surface Engineering, Vol. 5, No. 1, 2023, 2202002.